
This is an electronic reprint of the original article.
This reprint may differ from the original in pagination and typographic detail.

Dagyte, Vilgaile; Anttu, Nicklas

Modal analysis of resonant and non-resonant optical response in semiconductor nanowire arrays

Published in:
Nanotechnology

DOI:
[10.1088/1361-6528/aaa26](https://doi.org/10.1088/1361-6528/aaa26)

Published: 11/01/2019

Document Version
Publisher's PDF, also known as Version of record

Published under the following license:
CC BY

Please cite the original version:
Dagyte, V., & Anttu, N. (2019). Modal analysis of resonant and non-resonant optical response in semiconductor nanowire arrays. *Nanotechnology*, 30(2), Article 025710. <https://doi.org/10.1088/1361-6528/aaa26>

This material is protected by copyright and other intellectual property rights, and duplication or sale of all or part of any of the repository collections is not permitted, except that material may be duplicated by you for your research use or educational purposes in electronic or print form. You must obtain permission for any other use. Electronic or print copies may not be offered, whether for sale or otherwise to anyone who is not an authorised user.

PAPER • OPEN ACCESS

Modal analysis of resonant and non-resonant optical response in semiconductor nanowire arrays

To cite this article: Vilgail Dagt and Nicklas Anttu 2019 *Nanotechnology* **30** 025710

View the [article online](#) for updates and enhancements.



IOP | ebooks™

Bringing you innovative digital publishing with leading voices to create your essential collection of books in STEM research.

Start exploring the collection - download the first chapter of every title for free.

Modal analysis of resonant and non-resonant optical response in semiconductor nanowire arrays

Vilgaile Dągūtė¹  and Nicklas Anttu² 

¹NanoLund and Solid State Physics, Lund University, Box 118, SE-221 00 Lund, Sweden

²Department of Electronics and Nanoengineering, Aalto University, FI-00076 Aalto, Finland

E-mail: vilgaile.dagyte@ff.lth.se

Received 28 June 2018, revised 6 September 2018

Accepted for publication 22 October 2018

Published 9 November 2018



Abstract

Nanowire array solar cells have reached efficiencies where it becomes feasible to talk about creating tandem solar cells in order to achieve even higher efficiencies. An example of such a tandem solar cell could be a nanowire array embedded in a membrane and integrated on top of a Si bottom cell. Such a system, however, requires understanding and control of its interaction with light, especially to make sure that the low energy photons are transmitted to the bottom cell. The dependence of the optical response of a nanowire array on the nanowire length, diameter, array pitch, materials surrounding the nanowires, and absorption coefficient of the nanowire material is very strong and possibly resonant, indicating the complexity of the optical response. In this work, we use an eigenmode-based analysis to reveal underlying physics that gives rise to observed resonant and non-resonant behavior. First, we show that an effective refractive index can be defined at long wavelengths, where only a single mode propagates. Second, we analyze the origin of the resonant reflection when the next optical mode becomes propagating and can be ‘trapped’ in the array and interact with the fundamental mode. Additionally, we define two simple boundaries for the wavelength range of the resonant response: the resonances can only occur if there is more than 1 propagating mode in the array, and they disappear if the 1st diffracted order is propagating in the top or bottom material. Such resonance effects could be detrimental for tandem solar cells. We thus provide recommendations for tuning the geometry of the array and the nanowire materials in order to push the resonant regime to the absorbing regime of the nanowire, where absorption in the nanowires dampens the resonances. Finally, this work demonstrates the strength of an eigenmode-based analysis of the optical response of periodic nanostructures in terms of simplifying the analysis of a complex system.

Supplementary material for this article is available [online](#)

Keywords: III–V nanowire arrays, modal analysis, resonant reflection, tandem solar cells

(Some figures may appear in colour only in the online journal)

1. Introduction

III–V semiconductor nanowire arrays show promise for varying optoelectronic applications, including solar cells

[1–5]. However, the geometrical design of the nanowire array and its surroundings can have a strong impact on the optical response. In recent experiments, we performed reflection, transmission, and absorption measurements of 1.95 eV bandgap GaInP nanowire arrays embedded in a polymer membrane [6]. There, we observed a 40% reflectance peak below bandgap, which would be detrimental for tandem solar cells where transmission of low energy photons to the bottom cell is crucial. Such a reflectance peak is stronger even than



Original content from this work may be used under the terms of the [Creative Commons Attribution 3.0 licence](#). Any further distribution of this work must maintain attribution to the author(s) and the title of the work, journal citation and DOI.

the reflection from a planar III–V semiconductor interface, and was preliminarily assigned to resonant back-scattering from in-plane guided resonance modes in a nanowire-membrane sample. We proposed that the resonances show up only for nanowires embedded in a polymer, whereas they leak out when the array is standing on the substrate. In order to investigate this further, in this work, we use a quantitative optical-eigenmode-based analysis of the resonant and non-resonant optical response of nanowire arrays. In the method, we solve for the optical eigenmodes in the nanowire array and study how these eigenmodes are excited and how they propagate. Our analysis of the resonant response should be applicable for periodic nanostructures in general.

Resonant behavior is well-known in 1D and 2D non-absorbing dielectric gratings/arrays [7–23], and similar resonances have been used for enhancing the absorption in the weakly absorbing wavelength region of indirect transitions in Si nanowires [24, 25]. In this work, we focus on detailed, modal analysis of resonant reflection from nanowire arrays, and relate our results to previous studies in the discussion section in the end.

We find that for long wavelengths, only one optical eigenmode is propagating and defines the optical response. From the propagation constant of this eigenmode, we find an effective refractive index for the nanowire array, which simplifies the optics analysis considerably, since we can use the conventional Fresnel-equations for the nanowire array. Importantly, in this long-wavelength, single-mode regime, optical resonances don't show up. Instead, we see well-behaved interference oscillations, similar as in a conventional bulk thin-film, due to interference of the mode scattered between the top and the bottom of the array.

At a certain wavelength, which depends on the nanowire diameter and material, as well as the array pitch, a second propagating optical mode shows up. This optical mode corresponds to light that bounces between neighboring nanowires, and can lead to reflection (or absorption) resonances, where light travels in the array for a long time by reflecting between the top and bottom interface of the array. We show how also in this resonant regime, we can quantitatively analyze the optical response based on the propagating eigenmodes. Importantly, we find that both propagating eigenmodes are excited strongly. For even shorter wavelengths, additional diffracted orders in the bottom and/or top surrounding materials become propagating and our analysis shows how the optical eigenmodes of the nanowire array can leak into these diffracted orders, leading to a weakening and disappearance of the in-plane resonances.

With our optical-mode based analysis, we can predict and design the optical response of nanowire arrays more intuitively: we study what type of propagating eigenmodes are present for a given array geometry, and how these eigenmodes are excited, reflected, and transmitted at the top and bottom interfaces of the nanowire array. For example, when the nanowires are lifted into a membrane, the in-plane modes can be excited resonantly and dominate the optical response. We show that (1) decreasing the period of the array blue-shifts the whole resonant wavelength-range, (2) reducing the

diameter of the nanowires narrows the resonant wavelength-range by blue-shifting the long wavelength side, and (3) increasing the absorption coefficient of the nanowire material dampens the resonant excitation. Hence, by decreasing the period and/or the diameter, we can push the in-plane modes into the absorbing regime of the nanowires, leading to higher transparency for low energy photons, without reflection resonances of high-energy photons. Such geometry modification could be beneficial for e.g. nanowire-array-membrane-on-Si tandem solar cells [26]. Additionally, the in-plane waveguide modes lead to light-trapping, which can enhance absorption in otherwise weakly absorbing nanowires, which can be beneficial to, for example, Si nanowire solar cells [24, 25] or typically weakly absorbing nanowire intra-band photodetectors based on absorption in quantum wells [27].

2. Methods

In this work, we use two eigenmode-based methods for analyzing light scattering in a nanowire array—one that gives the exact solution of the full 3D light-scattering problem and one that simplifies the analysis. In general, we expand the electromagnetic field in terms of the diffracted orders in the homogenous region on top of the array, as well as in the region below the array. In the nanowire array region, we expand the field in terms of the corresponding eigenmodes of the nanowire array (see figure S1 for a schematic, which is available online at stacks.iop.org/NANO/30/025710/mmedia). In both methods, we first solve Maxwell equations for eigenmodes in the nanowire array and apply boundary conditions in order to calculate scattering of each mode at each interface. With knowledge of the modes in all parts of the system, a scattering matrix can be formed, which describes the connection between the incident and the outgoing fields. In the case of a single z -invariant region, like the nanowire array, the scattering matrix can actually be expressed analytically as given by equations (S17) and (S18) in the supplementary information. In the more complicated case of several layers (e.g. figure 6), the scattering matrix needs to be formed fully numerically, for example through iteration [28]. This constitutes the full scattering matrix method (SMM) [28], where the scattering matrix includes in principle contribution from all the optical modes of the nanowire array, both the propagating and the evanescent ones. This full scattering matrix gives the exact solution to the 3D light-scattering problem.

However, as explained in the supplementary information, we can simplify the system further by considering only the propagating modes without losing accuracy in calculation of the reflectance and transmittance. Such propagating mode analysis works well when the least decaying evanescent modes show a decay length much shorter than the nanowire length. If there are evanescent modes with longer decay lengths, such modes might need to be included in order to increase the accuracy of the calculation (see supplementary information, figure S3). This second method we call the propagating mode analysis method and it allows us to

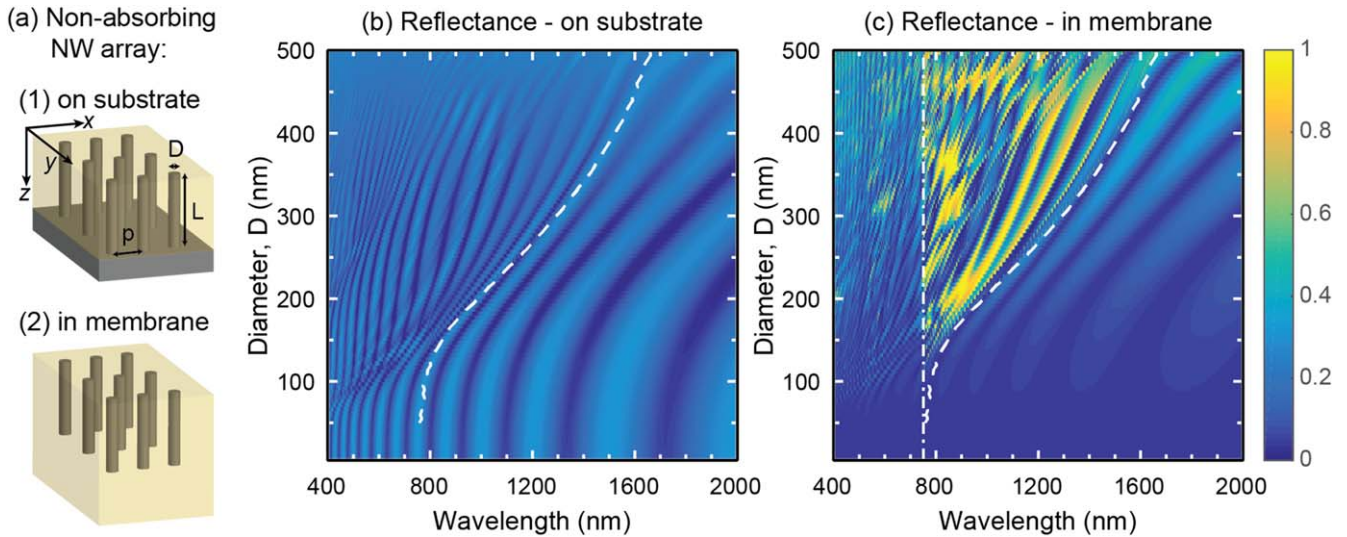


Figure 1. (a) Geometry of a non-absorbing nanowire array ($n = 3.5$) embedded in a polymer ($n = 1.5$) on a semi-infinite (1) substrate ($n = 3.5$), or (2) a polymer ($n = 1.5$), with air ($n = 1$) above the array in both cases. (b), (c) Dependence of the reflectance spectra on the diameter for a nanowire array (b) on a substrate, and (c) in an extended polymer membrane for light incident at normal angle from the top air side. The array geometry is set to $p = 500$ nm and $L = 2000$ nm. Resonant behavior is observed between two cutoffs in (c): the 1st diffracted order cutoff on the left (dashed–dotted line) and the 2nd mode cutoff on the right (dashed line). In (b), the cutoff for the 1st diffracted order is at 1750 nm, thus resulting in a lack of resonant regime as described in the main text.

simplify the analysis of the mode excitation and interaction, similarly as employed by Lalanne *et al* for a 1D line grating [19].

In addition, we have verified our analysis towards full 3D optics modeling in COMSOL Multiphysics (version 5.3a [29]) that solves the Maxwell equations directly in real space, without relying on analysis through optical eigenmodes (see supplementary information figure S6 for the level of convergence used in this study between the two methods). Such modeling based on the Maxwell equations has shown good agreement with measured spectra of nanowire arrays [30].

Note that there is a close relation between the optical eigenmodes we solve for and the modes solved for in the case of a photonics crystal bandstructure: the modes we solve for at normal incidence correspond to the modes at the Γ point of the photonic crystal consisting of infinitely long nanowires. However, since we consider a scattering problem, we must also solve for the evanescent modes at a given wavelength (or equivalently, frequency), whereas for the photonic crystal bandstructure, only the propagating modes with a real-valued propagating constant k_z^α are solved for (see supplementary information for additional technical details). Note that we consider in our modeling only the eigenmodes that can be excited due to the array symmetry in combination with the polarization and incidence angle of the incident light.

Unless mentioned otherwise, the nanowire array is non-absorbing and has geometry defined by pitch $p = 500$ nm (square array), diameter $D = 180$ nm, and length $L = 2000$ nm, with refractive index of $n = 3.5$ for the nanowires—a typical value for III–V semiconductors. The geometry was picked to be suitable for nanowire array solar cells, based on previous experiments [4]. The nanowire array is embedded in a polymer with refractive index of 1.5, as shown in figure 1(a), and is surrounded by air ($n = 1$) at the top side.

For most of this article, a semi-infinite layer at the bottom is made of polymer ($n = 1.5$) as shown in figure 1(a) (2). From here on, we will refer to the material just above (below) the nanowire array as the top (bottom) region.

We consider x -polarized, normally incident light (that is, with k -vector parallel to the nanowire axis, which is parallel to the z axis) from the top air side. The normally incident light maximizes the projected area of the array to the incident light, which maximizes the efficiency potential of a solar cell under direct solar illumination. Note, however, that the resonant response identified in this work shows up for a broad range of incidence angles and is not exclusive to normal incidence (supplementary information figure S7).

From the eigenmode analysis, we find two types of modes: those modes with real-valued propagation constant $k_z^\alpha = \text{Re}(k_z^\alpha)$, which we call propagating modes, and those that show evanescent decay, that is, modes where $\text{Im}(k_z^\alpha)$ is non-zero, which we call evanescent modes. Both types of modes are excited at the top and bottom interfaces of the array, but while the propagating modes propagate through the nanowire array without decay, the evanescent modes decay exponentially into the nanowire array.

Importantly, for each mode in the nanowire array except for the fundamental mode (which corresponds to the HE_{11} fiber mode in the individual nanowires [31]), a cut-off wavelength $\lambda_{\text{cutoff}}^\alpha$ (where α is the mode number) can be found beyond which the mode becomes evanescent (see supplementary information figures S8 and S9). Note that the 2nd mode cutoff $\lambda_{\text{cutoff}}^{\alpha=2}$ is especially important in this work, because it defines the boundary between a multi-mode and a single mode regime. This cutoff will be indicated in several figures.

Similarly, in the bottom and top regions, we find the diffracted orders, which are the optical eigenmodes in those

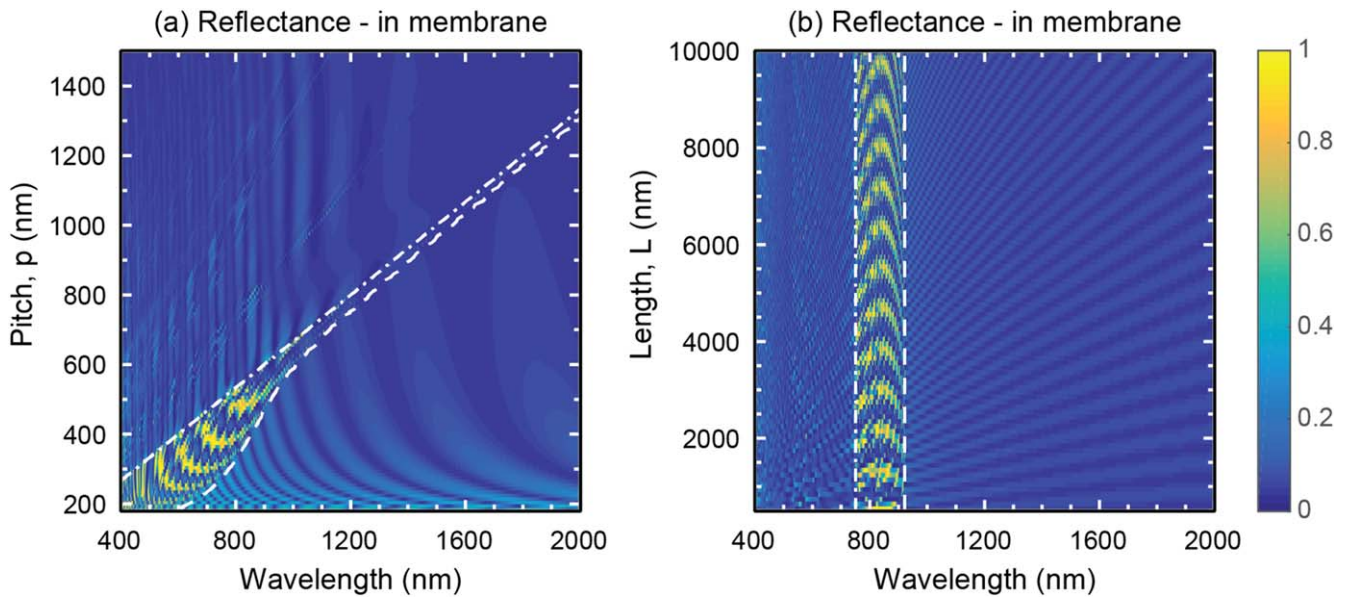


Figure 2. Reflectance spectra as a function of (a) pitch and (b) length. The non-varied geometrical parameters are kept at $p = 500$ nm, $D = 180$ nm, and $L = 2000$ nm. The refractive indices are 1 (air) above the array, 1.5 (polymer) between and below the nanowire array, and the nanowires have $n = 3.5$. Resonant behavior is observed between two cutoffs: the 1st diffracted order cutoff in the polymer underneath the nanowire array (dashed–dotted line) and the 2nd mode cutoff (dashed line).

regions (see supplementary information for details). Hence, also they show a cut-off wavelength where the diffracted order changes from a propagating to an evanescent one at longer wavelengths. For normally incident light, the cut-off for the first diffracted order, beyond the zeroth order that propagates (for all wavelengths) at normal angle, is given by $\lambda_{\text{cutoff,bot(top)}} = pn_{\text{bot(top)}}$, where $n_{\text{bot(top)}}$ is the refractive index of the bottom(top) material respectively.

3. Results

3.1. Geometry dependence

To begin with, we compare the reflectance of a nanowire array embedded in a polymer: first with that of a substrate under the array (figure 1(b)), and then with that of a polymer under the array (figure 1(c)). Corresponding figure for an as-grown nanowire array on a substrate with air between the nanowires is shown in supplementary information figure S10.

The main point to highlight is the presence of resonant reflectance in figure 1(c) reaching 100% reflectance values, unlike the 30% reflectance seen for the nanowire array on a substrate in figure 1(b). This difference is caused by the resonant excitation of in-plane array modes when there is no substrate to leak into. Note that the resonant reflectance in figure 1(c) is bounded by white lines, where the dashed–dotted line indicates the 1st diffracted order cutoff in the polymer ($\lambda_{\text{cutoff,bot}} = pn_{\text{bot}}$), whereas the dashed line indicates the 2nd mode cutoff in the nanowire array, obtained from the analysis of the eigenmodes. For figure 1(b), the 1st diffracted order cutoff in the substrate is at a wavelength of 1750 nm that is longer than the 2nd mode cutoff, which thus explains the lack of the resonances.

Before going into detailed analysis, we illustrate how reflectance spectra for nanowire arrays in a membrane depend on the diameter (figure 1(c)), the pitch (figure 2(a)), and the length (figure 2(b)). Again, we see that resonances lie between the two cutoff lines, which thus can be used as a simple and fast method to estimate the location of the resonant regime without solving the full 3D light-scattering problem. Knowing how the resonances shift with geometrical parameters allows us to design and optimize desired properties of nanowire arrays. Towards the end of this paper, we will give an example where such tuning is needed.

It is worth noting that the length dependence, on the first look, shows an unexpected behavior for the resonant regime—we see curved, hill-like structures, whereas outside the resonant regime we see a positive gradient of the fringes (which is expected, because if the k -vector of the light decreases with increasing wavelength, then the length needs to increase in order to keep the phase gathered during a roundtrip through the nanowire array constant and thus to stay on a specific interference fringe). The pattern in the resonant regime is actually formed by interference between two propagating modes, as analyzed in the next section.

3.2. Propagating mode analysis

To understand what is happening in this system, we choose a fixed nanowire array geometry with $p = 500$ nm, $D = 180$ nm, and $L = 2000$ nm and plot the reflectance spectrum in figure 3(a) (this corresponds to a specific horizontal linecut from any one of figure 1(c) or figures 2(a), (b)). Analysis of the spectrum obtained with the full 3D optics modeling is complicated due to the inclusion of a large number of modes (on the order of 100 modes were used for numerical convergence, but most of these modes are evanescent and affect

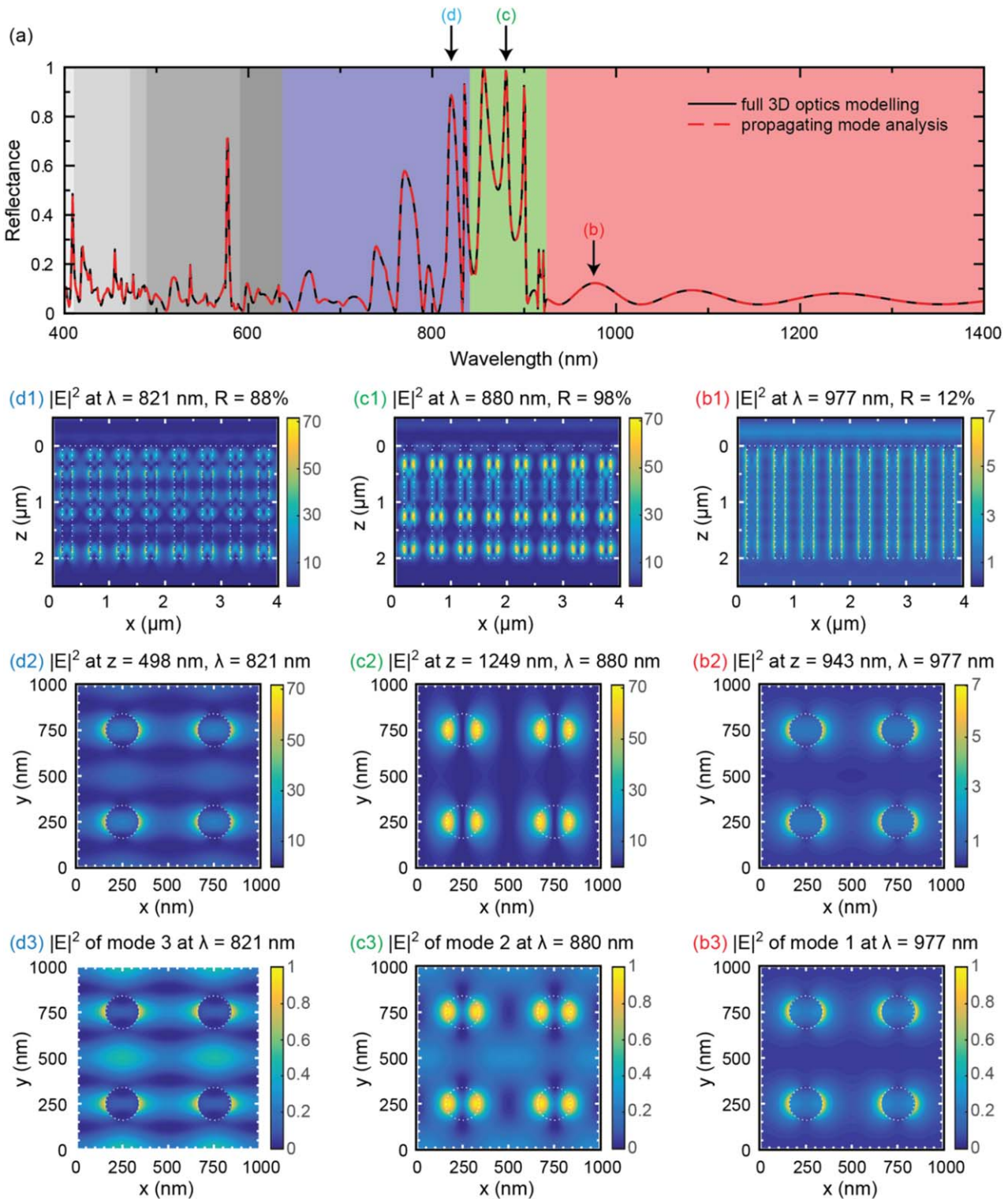


Figure 3. (a) Reflectance spectrum of normally incident light from the top side for a nanowire array with $p = 500$ nm, $D = 180$ nm, and $L = 2000$ nm in membrane, as calculated by the SMM (black line), and by the propagating mode analysis using only the propagating modes (red dashed line). The refractive indices are 1 (air) above the array, 1.5 (polymer) between and below the nanowire array, and the nanowires have $n = 3.5$. The different color areas indicate the number of modes that propagate in that wavelength range: single mode (red), two modes (green), three modes (blue), etc. (b1)–(d1), (b2)–(d2) illustrate the total field distribution normalized to the $|E|^2$ of the incident light in air, as calculated by COMSOL Multiphysics for the same geometry and the specific wavelengths as indicated by arrows in (a). Eigenmode field plots, normalized to their maximum value, are given for mode 1 of the single-mode regime (b3), mode 2 of the 2-mode regime (c3), and mode 3 of the 3-mode regime (d3) for the same wavelengths as indicated by the arrows in (a). The white dotted lines outline the interfaces between the nanowire array and the polymer (and the top air interface in the side view in (b1)–(d1)).

only the interaction and optical near-field at the top and bottom interfaces of the array). Therefore, to simplify the analysis, we turn to the propagating mode analysis method (see Methods section above and supplementary information for more details of the method). There, we use only the propagating modes, which are expected to dominate the transport of optical intensity from the top region to the bottom region, unless one, or several, of the evanescent modes have a decay length comparable to the nanowire length, in which case such modes need to be included as well (see supplementary information figure S3). (Note, however, that we need knowledge of all the ~ 100 modes used in the full 3D modeling to know how these propagating modes are reflected and transmitted at the top and bottom of the nanowire array). We observe a perfect agreement between the full 3D optics modeling (black line in figure 3(a)) and the multi-mode analysis method using only the propagating modes (red dashed-line in figure 3(a)). The different colors of the background in figure 3(a) mark the number of propagating modes in that wavelength range (red–1 propagating mode, green–2, blue–3, and so on). In this way, we simplify the analysis of how modes interact and create observed optical effects. For example, we can immediately see that the strongest resonances lie in the wavelength range with 2 and 3 propagating modes.

Next, we look at the total field distributions, as calculated with COMSOL Multiphysics for three specific wavelengths—reflectance peaks in one, two and three propagating mode regimes, as indicated by letters (b), (c), and (d) respectively in figure 3(a). The total field distributions at these wavelengths are shown for nanowire axial cross sections through the center in figures 3(b1)–(d1), and for radial cross sections at a specified position (z) along the nanowire, which displays a high total field value (figures 3(b2)–(d2)).

The single propagating mode in figures 3(b1), (b2) is the array equivalent of the HE_{11} fundamental fiber mode, which is typically localized to the individual, constituent nanowires of the array (unless the inter-wire distance becomes small between the nanowires so that the modes start to overlap considerably between the neighboring nanowires, or if D/λ becomes small so that the field is expelled from the individual nanowires [32]). When a second propagating mode is introduced (figures 3(c1), (c2)), the complexity of the total field increases due to the interaction between the multiple modes. Thus, analysis of such multiple modes becomes difficult. However, these total field distributions immediately illustrate a strong field enhancement in the resonant range. In the single mode regime, the field is enhanced around 7 times compared to the field of the incident light in the air (figure 3(b1)), whereas for the chosen resonance peak in the 2 mode regime, the enhancement is around 70 times (figure 3(c1)), illustrating the resonant response. Note that the field enhancement is weaker in the dips (not shown), indicating a weaker resonant response.

If we look at the radial cross section of the total field distributions, we can actually recognize resemblance to the eigenmodes of the system, where eigenmodes 1, 2, and 3 are shown in figures 3(b3)–(d3) respectively, each obtained for

the same wavelengths as the corresponding radial cross section of the total field distributions in figures 3(b2)–(d2). Thus, the radial cross sections of the nanowires at the chosen position along the nanowire with high total field values seem to be dominated by a specific eigenmode. (Note, however, that at other positions along the nanowire axis, the radial field distributions vary.) Specifically, as mentioned before, we can immediately identify the eigenmode 1 to be related to the HE_{11} fundamental mode. The type of the other modes is not as obvious. However, each mode approaches a corresponding hybrid HE or EH fiber mode localized to the individual nanowires at short wavelengths (see supplementary information figure S8 and note that we do not excite transverse electric and transverse magnetic fiber modes at normal incidence).

If we look more carefully at the single propagating mode regime, we observe familiar Fabry–Perot oscillations due to multiple scattering of the mode between the top and the bottom of the array. From the propagation constant of this eigenmode, we identify an effective refractive index for the nanowire array, $n_{\text{eff}} = n_{\alpha=1} = k_z^{\alpha=1}/(2\pi/\lambda)$, where $n_{\alpha} = k_z^{\alpha}/(2\pi/\lambda)$ is the effective refractive index of mode α with propagation constant k_z^{α} , and λ is the wavelength. When we use this n_{eff} in standard equations for thin-films, which include the Fresnel reflection and transmission coefficients, we find good agreement with the full 3D modeling from SMM at long wavelengths (see supplementary information, figure S4(b)). Thus, n_{eff} simplifies the optics analysis considerably at the long wavelengths, since we can use the conventional Fresnel-equations. However, at shorter wavelengths, the spectra using such an effective refractive index deviate from those of the full 3D modeling. This discrepancy indicates that it might not be possible to define an effective refractive index that produces exactly the observed behavior at these shorter wavelengths, even before the second mode becomes propagating.

At a certain wavelength, which depends on the nanowire diameter, material, and the array pitch, the second propagating optical mode shows up. This optical mode corresponds to light that bounces between the wires, and can lead to reflection resonances, where light travels in the array for a long time by reflecting between the top and bottom interfaces of the array. We quantitatively analyze the optical response in this wavelength range based on the propagating eigenmodes (see supplementary information figure S5). We find that both propagating eigenmodes are excited strongly: the resonant response couples to both eigenmodes. For even shorter wavelengths, additional diffracted orders in the top and/or bottom region become propagating and our analysis shows how the second propagating optical eigenmode in the nanowire array can leak/couple strongly into these higher-order diffracted orders, leading to a weakening and disappearance of the in-plane resonance. Alternatively, we can analyze how many roundtrips of light scattering between the top and the bottom interfaces need to be included for describing the optical response (see supplementary information figure S2). In the non-resonant single-mode regime, it is enough to include a single round-trip, in order to find good agreement

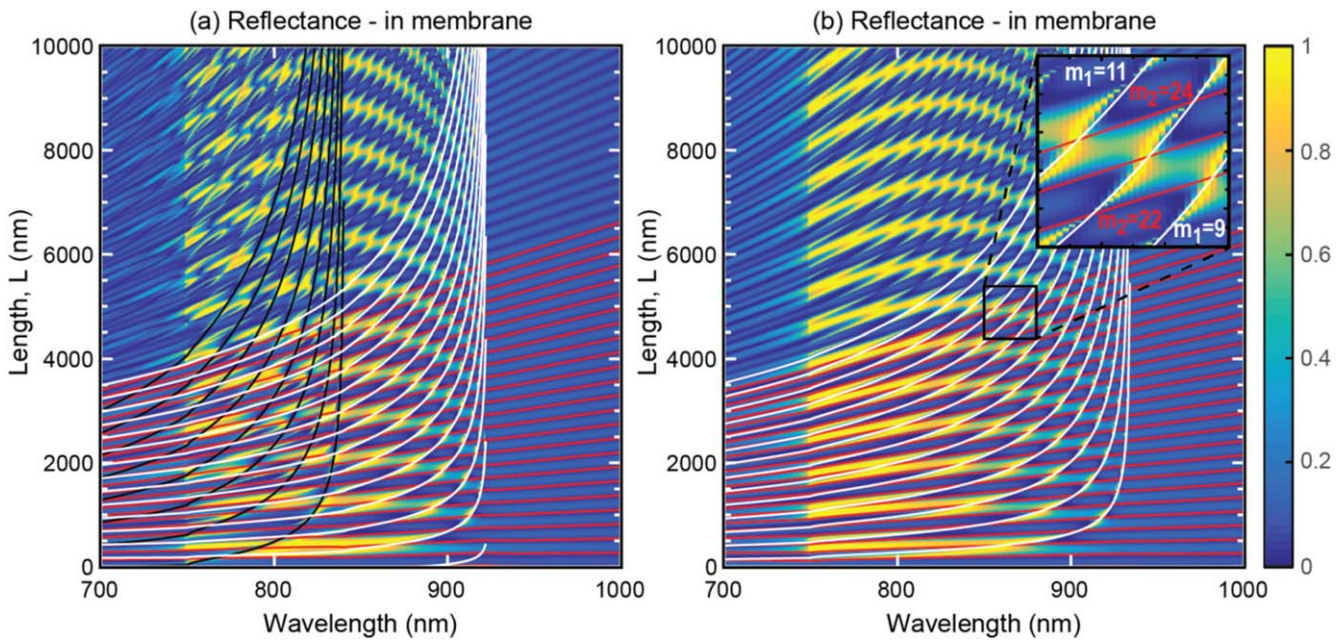


Figure 4. Analysis of the dependence of the reflectance spectra for $D = 180$ nm nanowires of varying length in terms of the constructive interference conditions [equation (1)]: (a) $p = 500$ nm, and we show the $2\pi m$ condition for the first 3 modes with $m = 0, 1, \dots, 24$ for mode 1 (red), $m = 0, 1, \dots, 14$ for mode 2 (white), and $m = 0, 1, \dots, 7$ for mode 3 (black); (b) $p_x = 500$ and $p_y = 400$ nm, and we show the $2\pi m$ condition for the first 2 modes, where the cut-off wavelength of the 3rd mode is blue-shifted to below $\lambda = 700$ nm and thus does not show up. $m = 1-24$ for mode 1 and $m = 1-14$ for mode 2 are visible. The $m = 0$ conditions are not observed in this system. The inset shows a zoom-in of the 850–880 nm wavelength and 4400–5400 nm length range, indicating that when $m_2 - m_1$ is odd, a broader reflectance maximum is observed. The refractive indices are 1 (air) above the array, 1.5 (polymer) between and below the nanowire array, and the nanowires have $n = 3.5$.

with the full 3D optics modeling. In contrast, in the resonant regime, we need to include roughly six roundtrips, which highlights the strong light scattering/trapping within the system at resonance.

If we look more carefully into the 2-mode regime, we find that the second mode gets strongly excited at some specific wavelengths (see supplementary information figure S5). In addition, both forward and backward traveling waves have similar excitation strength with coinciding peaks. These peaks correspond rather closely to the reflectance peaks. When the forward and backward traveling waves have similar excitation strength, it indicates zero transmission, which in the non-absorbing system leads to maximized reflectance (such similar excitation strength of forward and backward propagating version of the mode indicates a standing wave of the mode in the z -direction). Thus, the reflectance peaks seem to be caused by the array modes, in particular, the second mode that shows up after the fundamental one, because in the 3-mode regime, the positions of the strong excitation of modes and the reflectance peaks are not so well matched anymore.

Before continuing the discussion of how different modes interact with one another to create the resonances, we make a short detour to comment on the mode propagation directions, as it turns out to validate yet another simplification for the analysis. First, the eigenmode field plot in figure 3(d3) immediately indicates that mode 3 travels in y direction due to the observed standing wave pattern in the y direction. The other two modes do not show such a clear, directional behavior. So far, we have looked at a square array with a pitch p in both the

x and y directions, that is, when $p_x = p_y$. However, varying the pitch in x (p_x) and y (p_y) direction separately could reveal the propagation directions of each mode. If we change the pitch in the y direction for the x polarized incident light of this study, the cutoff wavelength as well as the propagation constant of mode 3 are strongly affected, whereas mode 2 is affected only slightly, and mode 1 even less (see supplementary information figures S9(a), (b)). On the other hand, if we vary the pitch in the x direction, we see that the propagation constant of mode 3 is relatively unaffected and mode 2 changes more, whereas mode 1 is still mostly unaffected (figure S9(c)). Through this quick analysis, we believe that mode 1 travels predominantly along the z axis (as expected for an optical fiber mode localized to the individual, constituent nanowires of the array [33]), whereas modes 2 and 3 show propagation also in the x - y plane, where mode 2 propagates predominantly in the x direction and mode 3 in the y direction.

Since the eigenmodes of the array are determined by the nanowire diameter and the array pitch, the nanowire length only affects the amplitude and phase of the excitation of the downward and upward propagating modes within the array. It is thus convenient to analyze the dependence of the reflectance spectra on the nanowire length to learn more about the interaction between the modes and how they are excited. In figure 4(a), we reproduce the dependence of the reflectance spectra on the nanowire length, previously shown in figure 2(b), but reduce the wavelength range in order to resolve more details. In addition, we also plot the lines corresponding to when the constructive interference condition

is met separately for mode 1 (red lines, $m = 0, 1, \dots, 24$), 2 (white lines, $m = 0, 1, \dots, 14$), and 3 (black lines, $m = 0, 1, \dots, 7$):

$$2\pi m = 2Ln_\alpha \frac{2\pi}{\lambda} + \varphi_{\text{bot}}^\alpha + \varphi_{\text{top}}^\alpha, \quad (1)$$

where m is an integer, L is the nanowire length, and $\varphi_{\text{bot}}^\alpha$ and $\varphi_{\text{top}}^\alpha$ are the phases from the reflection of the mode at the bottom and top interfaces. In figure 4, we observe a rather periodic behavior with nanowire length with peculiarly curved hill-like shapes for the resonances.

Before taking an even closer look at how the constructive interferences of different modes interact with one another, we simplify the problem even further. Since mode 3 travels predominantly in the y direction (for the x -polarized incident light we use), while mode 1 and 2 are mostly unaffected by the pitch in the y direction, we can slightly modify the array symmetry to push out the third mode from the resonant range. We thus plot the dependence of the reflectance spectra on the nanowire length, now, for a nanowire array with pitch $p_x = 500$ nm and $p_y = 400$ nm (figure 4(b)). This decrease of p_y blue-shifts the cut-off wavelength of the third mode (supplementary information figure S9(a)) without affecting the first and second modes significantly. Thus, now we have only 2 propagating modes in the resonant wavelength-range. However, note that the reflectance profile is very much similar to that obtained with 3 propagating modes before the decrease of p_y . This observation leads to the conclusion that the first two propagating modes create the resonant response, while the third mode only disturbs the resonances slightly (by creating additional fringes of low reflectance that cut through the reflectance-peak regions).

If we zoom in on the color plot in the 2 mode regime (figure 4(b) inset), we can analyze the cross-overs of the constructive interference conditions for mode 1 and mode 2. When the constructive interference conditions of the two modes meet, we get a reflectance maximum or minimum, depending on the phase of the modes at the bottom interface of the array. Hence, the very different dispersions of the two modes give the skewed lines in the length dependent reflectance spectra, where otherwise we would expect a redshift with increasing length if either mode by itself caused the resonant reflection fringes. More specifically, when $m_1 - m_2$ is odd, we get a maximum in reflectance, where m_1 (m_2) is the value of m in equation (1) for mode 1 (2). In this case, modes 1 and 2 are out of phase at the bottom interface, which results in suppressed transmission due to destructive interference between the modes in transmission. Further, the two modes are in phase at the top interface, which leads to in-phase reflection, giving resonant response since transmission is suppressed. Alternatively, if $m_1 - m_2$ is even, we get a dip in reflection. Furthermore, if the diameter is decreased to 100 nm, the coupling between the modes decreases, and, instead, mostly a narrow resonant reflection is seen, which seems to originate only from mode 2 (see supplementary information figure S11).

3.3. Absorbing materials—GaInP nanowires

So far, we have dealt with non-absorbing materials, which are relevant for semiconductor materials when the below bandgap region is of interest. For example, for tandem solar cells with nanowire membrane as a top cell, we would need high transmittance of the below bandgap photons. However, depending on the bandgap of the nanowire material and the array geometry, the absorption regime might overlap with the resonant regime. Thus, in figure 5, we show how the absorptance and the reflectance change with pitch for $\text{Ga}_{0.51}\text{In}_{0.49}\text{P}$ nanowires, with the complex refractive index taken from [34]. Note that figure 5(b) is similar to figure 2(a), but now, the nanowire refractive index is taken to be complex-valued and wavelength dependent, especially to include the material absorption of above-bandgap photons through the imaginary part of the refractive index. The bandgap of $\text{Ga}_{0.51}\text{In}_{0.49}\text{P}$ (1.85 eV) is marked with a vertical, dotted white line and shows a sharp cutoff for the resonances once absorption is possible. An additional example is shown with InP nanowires in supplementary information figure S12.

Instead of taking a specific absorbing material, we can define the nanowire refractive index to be $n_{\text{NW}} = 3.5 + i \times \text{Im}(n_{\text{NW}})$ for easier analysis compared to real materials that can show strong wavelength dependence in both $\text{Re}(n)$ and $\text{Im}(n)$. When we look at the absorptance and reflectance spectra as a function of $\text{Im}(n_{\text{NW}})$ (see supplementary information figure S13), we immediately notice that reflectance resonances disappear rather quickly with small $\text{Im}(n_{\text{NW}})$, that is, low absorption coefficient (where the absorption coefficient is given by $4\pi\text{Im}(n_{\text{NW}})/\lambda$). For example, $\text{Im}(n_{\text{NW}}) = 0.1$ is already large enough to fully dampen the resonances, which is to be compared with the typically higher values for III/V semiconductors (e.g., for 1.85 eV GaInP, $\text{Im}(n)$ goes from very close to 0 at just below the bandgap with a quick rise to 0.15 and then gradually increases towards 1 at 400 nm in wavelength). Thus, if the resonant regime overlaps with the absorption of a direct-bandgap III–V semiconductor, the resonances are expected to disappear.

We can use this disappearance of the reflection resonances with absorption to our advantage for tandem solar cell applications with a nanowire-array top cell: there, we want to transmit all below bandgap photons through the top cell, and resonant reflectance would be detrimental to the solar cell performance. In such a case, we could tune the geometry of the array to push the resonant regime into the absorbing regime of the nanowires (as discussed in the next section). Alternatively, we could imagine using resonant response to enhance absorption of weakly absorbing materials, for example, for photodetector applications.

3.4. Absorbing materials—GaInP nanowires with ITO

In the previous section, we mentioned that these optical effects are relevant for solar cell applications. One pathway for a nanowire-silicon tandem solar cell is to grow an array of nanowires separately on their native substrate, embed them into a polymer, and then peel them off the substrate [26]. This

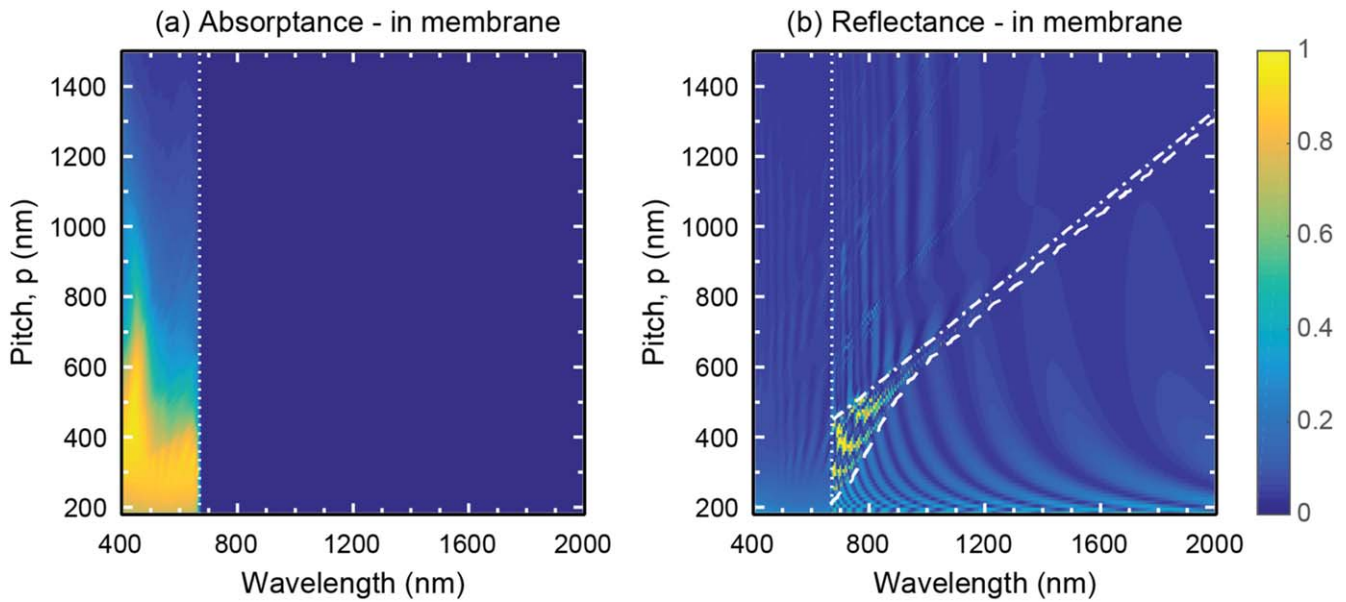


Figure 5. (a) Absorbance and (b) reflectance spectra as a function of pitch for a $\text{Ga}_{0.51}\text{In}_{0.49}\text{P}$ nanowire array in membrane, with $D = 180$ nm and $L = 2000$ nm. The refractive indices are 1 (air) above the array, 1.5 (polymer) between and below the nanowire array, and the nanowire refractive index is taken from reference [34]. The white lines are: the 1st diffracted order cutoff (dashed–dotted line), the single mode cutoff (dashed line), and the $\text{Ga}_{0.51}\text{In}_{0.49}\text{P}$ bandgap at 1.85 eV (dotted line).

results in a flexible solar cell that could be of interest on its own. Now, such a flexible solar cell will need transparent contacts, where we assume 50 nm planar ITO (indium tin oxide) layers on both sides of the array (for the optics modeling, we use the ITO refractive index values given in the supplementary information of [4]). Such a nanowire array solar cell is rather thin and fragile; therefore, we could either have a thicker polymer layer to have a flexible solar cell, or maybe put it on a glass sheet (figure 6(a)). If we look at the total transmittance and reflectance of the system, shown in figure 6(a1), we notice that in the resonant regime (shaded gray), the absorption in the weakly absorbing ITO is greatly increased, and when the absorption is low, resonant reflectance peaks appear. If we average over the resonant regime (750–887 nm in wavelength), we find $\text{mean}(A_{\text{ITO}}) = 0.23$, $\text{mean}(R) = 0.31$, and $\text{mean}(T) = 0.46$. These values can be converted to short circuit current (I_{sc}) values [4]: 1.8 mA cm^{-2} lost due to absorption in the ITO and 2.6 mA cm^{-2} lost due to reflection, as compared to the total 8.3 mA cm^{-2} available for Si in this wavelength region. If we look at the whole energy range from the Si bandgap (1.12 eV) to the GaInP bandgap (here 1.85 eV), then the loss due to the ITO absorption is 3.0 mA cm^{-2} and due to reflection 4.4 mA cm^{-2} , as compared to the total 23.7 mA cm^{-2} available for Si. This means that about 30% of the I_{sc} potential in the bottom Si cell would be lost, which is not acceptable for a tandem device.

However, as discussed above, modes can leak out into a high refractive index substrate. Hence, if we put this flexible solar cell directly on a Si solar cell (figure 6(b)), we would get rid of the resonances. This is illustrated in figure 6(b1), where the mean values over the resonant regime are now: $\text{mean}(A_{\text{ITO}}) = 0.08$, $\text{mean}(R) = 0.13$, and $\text{mean}(T) = 0.80$, which convert to 0.6 mA cm^{-2} for absorption in the ITO and

1.1 mA cm^{-2} for reflection in this wavelength range. In the whole range from Si to GaInP bandgap, the loss due to the ITO absorption is 1.7 mA cm^{-2} and due to reflection 3.3 mA cm^{-2} , which leads to 21% loss of I_{sc} for Si, where we can see significant reduction in both reflectance and absorbance losses compared to figure 6(a1). However, such remaining high losses, of course, are still not acceptable, to which we note that the 14% reflection loss could be further reduced with additional anti-reflection coatings [35], whereas the ITO recipe should be optimized further to reduce the ITO absorption in this wavelength range.

The resonances appear again if just a few hundred nanometers of glass/polymer spacer ($n = 1.5$) is introduced between the ITO and Si (figures 6(c), (c1)), because the modes cannot tunnel to the substrate anymore. The rough length-scale for tunneling can be understood by calculating the decay length of the 1st diffracted order in the spacer (see equation (S4) in the supplementary information for the evanescent decay of diffracted orders), which is 114.4 nm at $\lambda = 800$ nm and decreases with increasing wavelength, making the short wavelengths tunnel through easier than the longer ones. Looking at figure 6(c1), it seems that 400 nm of spacer fully prevents any tunneling. The same argument holds even if the ITO layer is made thicker (supplementary information figure S14).

These findings show that depending on the tandem solar cell design, we might face absorption and reflection resonance challenges. If we incorporate a tandem solar cell fully in the nanowire geometry, we would avoid such issues (see an example of a GaInP/InP nanowire tandem cell in supplementary information figure S15). Making an Esaki diode from the top nanowire array cell to the Si [37], or having a thin ITO layer without any other optical spacer also avoids the challenge. However, if we want to make a 4-terminal device with

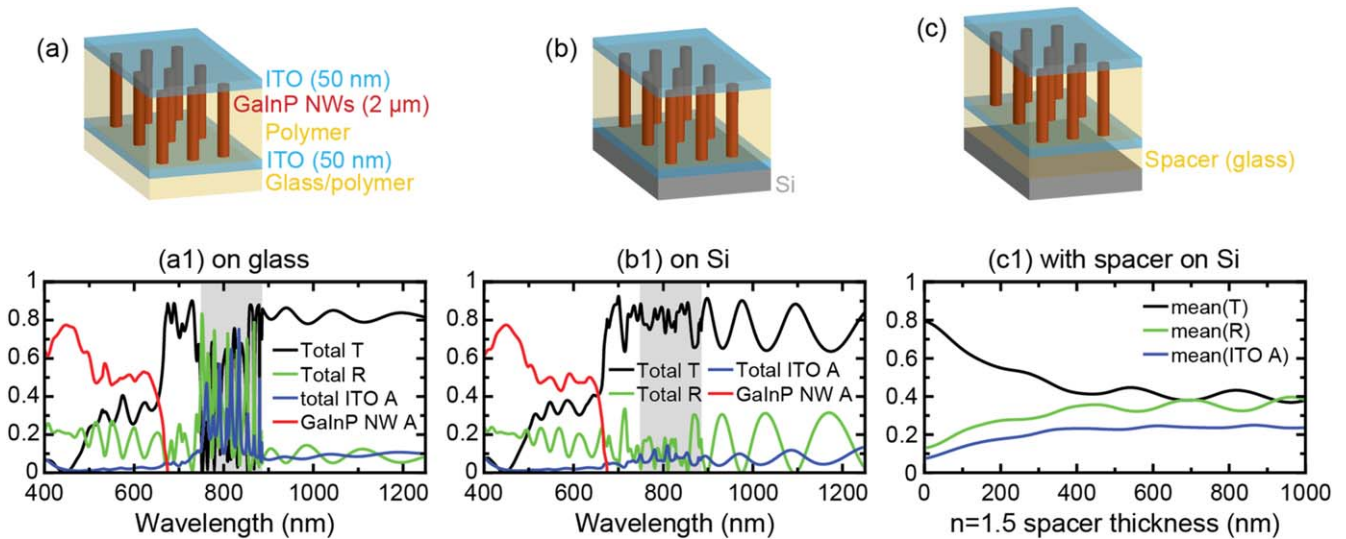


Figure 6. Geometries and the R , T , and A values for a $\text{Ga}_{0.51}\text{In}_{0.49}\text{P}$ nanowire array embedded in a polymer ($n = 1.5$), with 50 nm planarized ITO layers (n for ITO taken from the supplementary information of [4]) and on top of (a), (a1) semi-infinite glass/polymer ($n = 1.5$) layer, (b), (b1) semi-infinite Si substrate (n for Si taken from [36]), (c), (c1) variable thickness spacer layer ($n = 1.5$) before a semi-infinite Si substrate. The nanowire array geometry is $p = 500$ nm, $D = 180$ nm, and $L = 2000$ nm. The resonant regime (750–887 nm) in (a1), (b1) is shaded in gray, whereas (c1) shows values averaged over such a resonant wavelength-range for variable spacer thickness.

a spacer between the two cells, we need to turn to modifying the geometry of the array. As we saw from figures 1 and 2, we expect that nanowires should be packed tighter and have a smaller diameter in order to push the resonant regime into the absorbing regime of GaInP.

For $D = 180$ nm, it seems like $p < 220$ nm would be needed in order to push the resonances into the absorbing regime in the case of 1.85 eV bandgap. For such a bandgap of 1.85 eV, however, the optimal diameter for absorption in the nanowires is closer to 130 nm [31]. For that diameter, a pitch of $p < 360$ nm would be sufficient to push the resonances into the absorbing regime. Note, however, that the 1.85 eV bandgap is not the most suitable for a top cell with a Si bottom cell. This bandgap was chosen, based on available tabulated refractive index values for ternary compositions, to facilitate the optics modeling. In terms of absorption of light and current matching, we would prefer GaInP with a bandgap of 1.6 eV, which would make it easier to tune the geometry to mitigate the effect of the resonances, since the absorption edge would be red-shifted.

4. Discussion

Here, we relate our results to previous studies. The most relevant previous work, we identified, can be split according to 3 categories: (i) 1D [19, 22, 23] or 2D [16, 22–25] gratings/arrays, (ii) absorbing [24, 25] or non-absorbing [16, 19, 22, 23] materials, and (iii) analysis based on so-called guided resonance modes that propagate in the x - y plane [16, 22–24] or vertical eigenmodes that propagate in the z -direction like in our present work and [19, 25].

Regarding 1D and 2D array geometry, Ko *et al* [22] have shown that the principal features in the reflection spectra of a 2D array show good agreement with the corresponding 1D

grating spectra. The agreement is quantitative for small modulation strength. Our nanowire arrays tend to correspond to the strong modulation case. Therefore, analysis based on a corresponding 1D grating is expected to be relevant only qualitatively, and rigorous calculations of the 2D array are needed for the nanowire array structures of interest.

As we have shown, even moderately weak absorption can dampen the resonances very quickly. Thus, for direct bandgap III–V nanowires, the above-bandgap absorption leads to completely different response compared to the resonant response that can be found in the below bandgap, non-absorbing region. Si nanowires, on the other hand, are weakly absorbing due to the indirect bandgap for a large wavelength range (from approximately 600 to 1100 nm in wavelength). Therefore, resonant response can be observed even above the Si bandgap. However, previous work on Si nanowires has been focused on enhancing the weak absorption by absorption resonances [24, 25]. Therefore, the results of these Si nanowire studies are not directly applicable for elucidating how the resonant reflection shows up and how it affects the below bandgap transparency, which was the main focus of our present work.

Finally, the analysis method is an important topic that tends to divide the literature. Many articles, especially originating from a photonic crystal direction, analyze the resonances via guided resonance modes that can form standing waves in the lateral direction, that is, in the x - y plane [16, 22–24]. Others, including our present work, instead focus on the propagation along the nanowire axis, that is, along the z -direction, and use eigenmodes in that direction, which can show vertical, Fabry–Perot like array resonances [19, 25]. The two methods are complementary and highlight different aspects of the optical response. However, the analysis with eigenmodes propagating along the z -direction allows for a fully quantitative assessment of the excitation of all the modes by the incident light, without any fitting parameters [19, 25].

5. Summary

In this work, we have analyzed the resonant and non-resonant optical behavior of nanowire arrays embedded in a polymer. In particular, we have demonstrated the benefits of the eigenmode-based method that significantly simplified the analysis. From the eigenmode propagation constants, one can calculate the cutoff wavelengths and identify the wavelength-range for the resonant behavior without the full 3D optics modeling. Furthermore, just from the eigenmodes, we can tell where the actual resonant maxima show up by analyzing the interference conditions of two propagating modes. Finally, we have investigated how the resonances are influenced by the geometry and the properties of the surrounding materials. We have identified a potential issue for tandem solar cells with a nanowire-membrane cell on top of a Si bottom cell. If a spacer, or a thicker transparent contact layer, is used, resonant reflection can drastically reduce transmission of the low energy photons to the bottom cell. We suggest several directions to avoid this issue: (i) a thin transparent contact without a spacer layer, (ii) an Esaki diode joining the nanowire and bulk cells, (iii) both the top and bottom cells defined in a nanowire, and (iv) reducing the array pitch and the nanowire diameter in order to push the resonances into the absorbing regime of the top cell. Furthermore, introducing randomness in the array could be another direction for future investigations.

Acknowledgments

This work was performed partly within the NanoLund at Lund University, supported by the People Programme (Marie Curie Actions) of the European Union's Seventh Framework Programme (FP7-People-2013-ITN) under REA grant agreement No 608153 (PhD4Energy), European Union's Horizon 2020 research and innovation programme under grant agreement No 641023 (Nano-Tandem). We acknowledge support from the Academy of Finland through grant number 286920. This article reflects only the authors' views and the Funding Agency is not responsible for any use that may be made of the information it contains.

ORCID iDs

Vilgail  Dagty   <https://orcid.org/0000-0002-1740-8737>
Nicklas Anttu  <https://orcid.org/0000-0002-7626-5107>

References

- [1] Otnes G, Barrig n E, Sundvall C, Svensson K E, Heurlin M, Siefer G, Samuelson L,  berg I and Borgstr m M T 2018 Understanding InP nanowire array solar cell performance by nanoprobe-enabled single nanowire measurements *Nano Lett.* **18** 3038–46
- [2] van Dam D, van Hoof N J J, Cui Y, van Veldhoven P J, Bakkers E P A M, G mez Rivas J and Haverkort J E M 2016 High-efficiency nanowire solar cells with omnidirectionally enhanced absorption due to self-aligned indium–tin–oxide mie scatterers *ACS Nano* **10** 11414–9
- [3]  berg I *et al* 2016 A GaAs nanowire array solar cell with 15.3% efficiency at 1 sun *IEEE J. Photovolt.* **6** 185–90
- [4] Wallentin J *et al* 2013 InP nanowire array solar cells achieving 13.8% efficiency by exceeding the ray optics limit *Science* **339** 1057–60
- [5] Czaban J A, Thompson D A and LaPierre R R 2008 GaAs core–shell nanowires for photovoltaic applications *Nano Lett.* **9** 148–54
- [6] Anttu N, Dagty  V, Zeng X, Otnes G and Borgstr m M 2017 Absorption and transmission of light in III–V nanowire arrays for tandem solar cell applications *Nanotechnology* **28** 205203
- [7] Hope L L 1972 Theory of optical grating couplers *Opt. Commun.* **5** 179–82
- [8] Neviere M, Petit R and Cadilhac M 1973 About the theory of optical grating coupler-waveguide systems *Opt. Commun.* **8** 113–7
- [9] Vincent P and Neviere M 1979 Corrugated dielectric waveguides: a numerical study of the second-order stop bands *Appl. Phys.* **20** 345–51
- [10] Golubenko G, Svakhin A S, Sychugov V A and Tishchenko A V 1985 Total reflection of light from a corrugated surface of a dielectric waveguide *Sov. J. Quantum Electron.* **15** 886
- [11] Wang S S, Magnusson R, Bagby J S and Moharam M G 1990 Guided-mode resonances in planar dielectric-layer diffraction gratings *J. Opt. Soc. Am. A* **7** 1470–4
- [12] Magnusson R and Wang S S 1992 New principle for optical filters *Appl. Phys. Lett.* **61** 1022–4
- [13] Wang S S and Magnusson R 1993 Theory and applications of guided-mode resonance filters *Appl. Opt.* **32** 2606–13
- [14] Peng S and Morris G M 1996 Resonant scattering from two-dimensional gratings *J. Opt. Soc. Am. A* **13** 993–1005
- [15] Rosenblatt D, Sharon A and Friesem A A 1997 Resonant grating waveguide structures *IEEE J. Quantum Electron.* **33** 2038–59
- [16] Fan S and Joannopoulos J D 2002 Analysis of guided resonances in photonic crystal slabs *Phys. Rev. B* **65** 235112
- [17] Tikhodeev S G, Yablonskii A L, Muljarov E A, Gippius N A and Ishihara T 2002 Quasiguided modes and optical properties of photonic crystal slabs *Phys. Rev. B* **66** 045102
- [18] Ding Y and Magnusson R 2004 Resonant leaky-mode spectral-band engineering and device applications *Opt. Express* **12** 5661–74
- [19] Lalanne P, Hugonin J P and Chavel P 2006 Optical properties of deep lamellar gratings: a coupled Bloch-mode insight *J. Light. Technol.* **24** 2442–9
- [20] Magnusson R and Shokooh-Saremi M 2008 Physical basis for wideband resonant reflectors *Opt. Express* **16** 3456–62
- [21] Moitra P, Slovic B A, Gang Yu Z, Krishnamurthy S and Valentine J 2014 Experimental demonstration of a broadband all-dielectric metamaterial perfect reflector *Appl. Phys. Lett.* **104** 171102
- [22] Ko Y H, Shokooh-Saremi M and Magnusson R 2015 Modal processes in two-dimensional resonant reflectors and their correlation with spectra of one-dimensional equivalents *IEEE Photonics J.* **7** 1–10
- [23] Ko Y H and Magnusson R 2018 Wideband dielectric metamaterial reflectors: Mie scattering or leaky Bloch mode resonance? *Optica* **5** 289–94
- [24] Lin C and Povinelli M L 2009 Optical absorption enhancement in silicon nanowire arrays with a large lattice constant for photovoltaic applications *Opt. Express* **17** 19371–81
- [25] Sturmberg B C P, Dossou K B, Botten L C, Asatryan A A, Poulton C G, de Sterke C M and McPhedran R C 2011 Modal analysis of enhanced absorption in silicon nanowire arrays *Opt. Express* **19** A1067–81

- [26] Borgström M T *et al* 2018 Towards nanowire tandem junction solar cells on silicon *IEEE J. Photovolt.* **8** 733–40
- [27] Karimi M *et al* 2017 Intersubband quantum disc-in-nanowire photodetectors with normal-incidence response in the long-wavelength infrared *Nano Lett.* **18** 365–72
- [28] Anttu N and Xu H 2011 Scattering matrix method for optical excitation of surface plasmons in metal films with periodic arrays of subwavelength holes *Phys. Rev. B* **83** 165431
- [29] COMSOL AB 2017 Wave Optics Module User's Guide, COMSOL Multiphysics® v. 5.3a Stockholm, Sweden pp 38–46
- [30] Anttu N, Heurlin M, Borgström M T, Pistol M-E, Xu H Q and Samuelson L 2013 Optical far-field method with subwavelength accuracy for the determination of nanostructure dimensions in large-area samples *Nano Lett.* **13** 2662–7
- [31] Anttu N and Xu H 2013 Efficient light management in vertical nanowire arrays for photovoltaics *Opt. Express* **21** A558–75
- [32] Svensson J, Anttu N, Vainorius N, Borg B M and Wernersson L-E 2013 Diameter-dependent photocurrent in InAsSb nanowire infrared photodetectors *Nano Lett.* **13** 1380–5
- [33] Seo K, Wober M, Steinvurzel P, Schonbrun E, Dan Y, Ellenbogen T and Crozier K B 2011 Multicolored vertical silicon nanowires *Nano Lett.* **11** 1851–6
- [34] Schubert M, Gottschalch V, Herzinger C M, Yao H, Snyder P G and Woollam J A 1995 Optical constants of $\text{Ga}_x\text{In}_{1-x}\text{P}$ lattice matched to GaAs *J. Appl. Phys.* **77** 3416–9
- [35] Chen Y, Höhn O, Tucher N, Pistol M-E and Anttu N 2017 Optical analysis of a III–V-nanowire-array-on-Si dual junction solar cell *Opt. Express* **25** A665–79
- [36] Green M A 2008 Self-consistent optical parameters of intrinsic silicon at 300 K including temperature coefficients *Sol. Energy Mater. Sol. Cells* **92** 1305–10
- [37] Yao M, Cong S, Arab S, Huang N, Povinelli M L, Cronin S B, Dapkus P D and Zhou C 2015 Tandem solar cells using GaAs nanowires on Si: design, fabrication, and observation of voltage addition *Nano Lett.* **15** 7217–24